Three-Dimensional Representation and Analysis of Brain Energy Metabolism

LYNDON S. HIBBARD, JAMES S. MCGLONE,* DONALD W. DAVIS, RICHARD A. HAWKINS

Quantitative autoradiography of brain glucose metabolism has been combined with digital image processing to represent the brain as a three-dimensional (3-D) reconstruction of brain energy use. Autoradiographs contain enormous amounts of potentially useful data, but conventional analyses, based on tedious manual methods, can sample and analyze only a small portion of this information. Computer 3-D reconstruction provides a mechanism for observing and analyzing all the data; therefore, a system of computer programs was developed for this purpose. The programs use digital imaging methods for image registration, superimpose whole brain data sets, and allow resampling of the 3-D data in arbitrary planes for pixel-by-pixel comparisons among multiple 3-D sets. These programs operate on the mathematical properties of the images alone, obviating the need for manual image alignment. Various statistical analyses can be applied to the data directly to study the patterns of metabolic changes in different experiments. The system is applied to data from experiments on the influence of injectable anesthetics on cerebral glucose metabolism.

CEREBRAL FUNCTION IS DEPENDENT ON NEURONAL ORGANIZATION and metabolic activity. The wide variety of behaviors exhibited by living creatures is reflected in the anatomic complexity of the brain, where the relations between the regional organization of nerve cell groups and function have been identified by descriptive neuroanatomy. Likewise, the brain exhibits a complex metabolic pattern. This pattern is revealed by quantitative autoradiography of the cerebral metabolic rate of glucose utilization (CMRglc), which is a reflection of the rate of the energy consumption required to support cellular activity throughout the entire brain (*1*). Quantitative autoradiography of CMRglc permits the examination of anatomy and function simultaneously and in great detail. Its high resolution requires computer methods in order to fully utilize the immense amount of data available; often there are millions of individual measurements per rat brain. Computer reconstruction of the brain in three dimensions provides a mechanism for organizing and comparing data from different experiments in full detail over the entire brain. We have developed a reconstruction program system that uses digital image processing to minimize the labor and operator bias inherent in interactive imaging methods. These programs can be applied to a variety of measurements in addition to CMRglc, including studies of blood flow, blood-brain barrier transport, and receptor mapping. At present the techniques have been most widely employed in experiments on CMRglc in rats. This application is therefore used for illustration.

The measurement of CMRglc by quantitative autoradiography is relatively straightforward. The essential requirement is a tracer of glucose metabolism that generates a labeled product that remains in the brain at the site of metabolism for the experimental period. There are two distinctly different types of tracers currently being used: fully metabolizable glucose labeled in a specific position (*2*) and glucose analogs such as deoxyglucose (*3*). In our laboratory, we prefer the use of [6-^{14}C]glucose because the time of the experiment can be kept short, and the kinetics are considerably simpler. Nevertheless, both types of glucose tracers are employed in a similar manner. Each is introduced into circulation for a period of time (5 to 10 minutes for [6-^{14}C]glucose or 45 minutes for [^{14}C]deoxyglucose); during this period frequent blood samples are taken for the determination of circulating glucose and radioactivity concentrations. At the end of the experiment, the rat is killed, its brain is sectioned, and the sections are placed against x-ray film to produce autoradiographs. Typically, in our laboratory, 40-μm-thick sections are cut through the entire brain, yielding about 560 sections. Usually, only one section in four is saved and exposed to x-ray film. When developed and digitized at 100-μm resolution, each image contains from 10,000 to 15,000 individual measurements of CMRglc, or about 1.5 million data points for the whole brain. The radioactivity of the sections is quantitated by comparing the optical densities of the x-ray film images with the optical densities produced by a set of calibrated standards. The amount of radioactivity in any given tissue volume is a function of its CMRglc, the circulating glucose and tracer concentrations, and time. Thus, all experimental variables from which CMRglc is calculated are measured.

In most laboratories, autoradiographs are analyzed manually by measuring the optical density at arbitrary points in 50 to 100 neural structures. The results are reported as sets of CMRglc values corresponding to these optical density measurements. Thus, only a small fraction of the immense amount of autoradiographic data available from each experiment is examined. Comparison of different experiments relies on the reproducibility of manual measurement and the extent to which a single measurement accurately represents the metabolism of an entire neural structure. The potential for bias

L. S. Hibbard is in the Departments of Radiology and Anesthesia, J. S. McGlone is in the Department of Bioengineering, D. W. Davis is in the Department of Anesthesia, and R. A. Hawkins is in the Departments of Anesthesia and Physiology, Pennsylvania State University College of Medicine, Hershey, PA 17033.

*Present address: Siemens Medical Systems, Inc., 1515 Main Street, Pittsburgh, PA 15215.

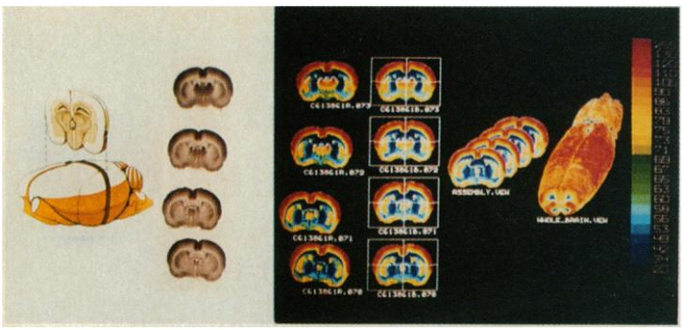

Fig. 1. The steps in analyzing and reconstructing a rat brain are shown from left to right. (i) First the brain is sectioned. (ii) The sections are placed against x-ray film to produce images. (iii) The film is digitized by a computer driven microdensitometer; CMRglc is calculated for each individual pixel, color-coded, and displayed. (iv) Images are rotated and translated to the center of a fixed coordinate system. Finally, (v) the images are reassembled as a 3-D reconstruction in a defined coordinate axes system.

in this approach is usually accepted as a suitable compromise between subjective undersampling and the interpretive difficulty inherent in such large bodies of data. A second, perhaps more important, problem with conventional methods is that the response of the central nervous system to a stimulus is seldom localized to one or even a few structures. We have found in a variety of studies that the response is much more widespread, in some cases affecting virtually every point in the brain to a greater or lesser degree. Therefore, to fully characterize experimental changes, it is necessary to examine the entire data set.

Reconstruction of autoradiographic data provides a method for comparing different experiments, and for combining similar experiments to form average and standard deviation data sets (*4*). Average reconstructions can be compared to each other point-by-point, and the differences identified on the basis of probable significance. Also three-dimensional (3-D) reconstructions easily lend themselves to multivariate statistical methods such as principal component analysis.

Reconstruction Overview

Our overall goal has been to make the computer do as many of the operations as possible. Although there remain some tasks that must be done by the operator, these have been restricted to those involving manual handling of objects (for example, tissue sectioning) or to those tasks that involve objective decisions (for example, expunging external artifacts). A typical sequence of events leading to the reconstruction of a single brain is illustrated in Fig. 1. (i) Brains are sectioned and high quality autoradiographs are produced. (ii) The autoradiographs are scanned with a computer-operated microdensitometer (Optronics P-1000). The data, stored in optical density files, are converted to CMRglc values, based on other experimental measurements unique to the experiment and animal. (iii) The images are displayed. At this stage artifacts in the field surrounding the image are removed, because these can interfere with subsequent alignment operations. (iv) The images are aligned by using one or both of the algorithms described below so that they are in register with the other images in the same serial set. (v) The images are combined and displayed, as in the stereogram of whole brain shown in Fig. 1.

There are a variety of other operations that may now be performed on the 3-D reconstructions: The whole brain can be resampled either axially or sagittally to reveal internal structures; several brains can be combined into a group-average brain where each point represents the mean and has a standard deviation; and analytic statistical methods can be applied to the whole brain or to selected axial or sagittal planes. These routines, written in FORTRAN and running on DEC VAX 11/780 and Micro VAX II computers and AED 1024 color terminals, provide a powerful collection of tools to examine brain function (*5*).

Preparation of Images

The experimental procedures for conducting CMRglc experiments, for making sections, for making autoradiographs and digitizing them, and for converting optical density values to CMRglc are described elsewhere (*2*). For our description we shall begin with the files representing digitized images that have been converted to rates of glucose utilization. Although it is convenient to discuss these files as "images," in reality they consist of a large number of individual rate determinations. These are grouped into discrete levels and displayed on the color terminal for the sake of convenience. Our display programs enable the experimenter to assign color to a rate value arbitrarily or by equalization. Histogram-equalized rate-to-color assignments result in approximately equal numbers of pixels in each of the displayed colors; such an assignment best uses the dynamic range of the colors to maximize the overall contrast in the image. Further, a single equalized assignment may be calculated for all the images in a serial set. This usually provides adequate viewing contrast within each single image as well as the means for comparisons with the other images in the set. Here we use only one assignment for rate data, which was derived from many serial sets, to provide a common visual reference.

Before submitting the image files to alignment and assembly routines some editing may be required. Each image is scrutinized for artifacts outside the image field (for example, dust or a strip of dura that became detached and projects away from tissue margin). These artifacts can interfere with the image alignment and scaling programs. Therefore, interactive graphics programs were written to allow the investigator to identify and remove them.

Image Registration

A fundamental problem confronting all 3-D reconstructions is that of image registration. In most of the reconstructions reported in the literature, registration involves the interactive matching of artificially introduced fiducial marks or image features common to

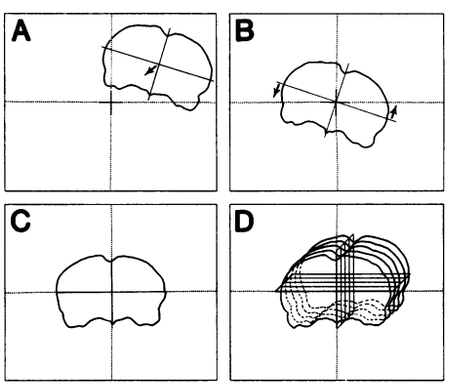

Fig. 2. Image alignment by the principal axes method. After scanning, the images must be translated and rotated to be placed in register. In the principal axes method, the center of mass (centroid) and principal axes are calculated for each image (**A**). The image is translated to a predetermined set of coordinates by using the centroid as the image reference point (**B**). The amount of rotation is determined from the angle between the long principal axis and the horizontal reference axis. The image is then rotated so that the principal axis is coincident with the horizontal axis (**C**). Many sections are assembled into a 3-D reconstruction with their centroids as the common reference point (**D**).

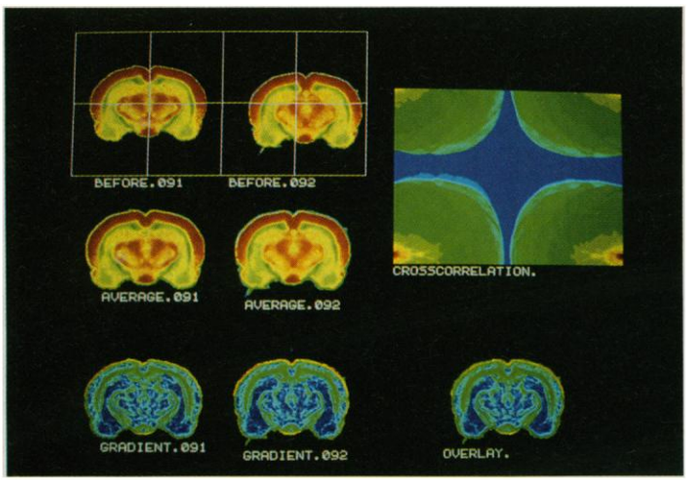

Fig. 3. Image translation by the cross-correlation method. Generally image misalignments have both translational and rotational components, which must be corrected in separate steps of an iterative procedure. Here correction for a translational misalignment is demonstrated for images BEFORE.091 (aligned) and BEFORE.092, where image 92 has been artificially displaced down and to the right as shown. The correct displacement up and to the left can be determined from the location of the maximum of the cross-correlation function. First the images are smoothed (second row, left) and the features enhanced by a gradient operator (third row, left). The cross-correlation function is calculated for the smoothed, edge-enhanced images with the fast Fourier transform (upper right). The input gradient images are shown superposed after the translation (lower right).

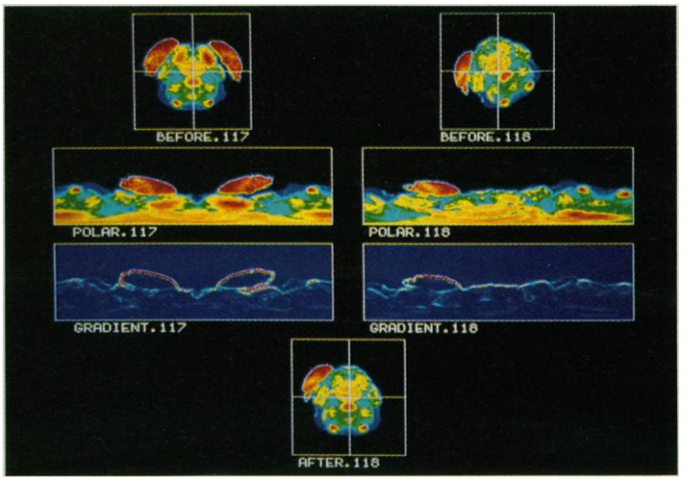

Fig. 4. Application of polar resampling to irregular sections. (**Top row**) Two adjacent sections. The one on the left was successfully aligned by the principal axes method, but the one on the right is missing a portion of the occipital cortex, hence, both the angle of rotation and the center of mass are aberrant. In this instance both sections were sampled around 360° at 2° increments. (**Second row**) Untreated polar-resampled versions of the sections. (**Third row**) The smoothed, gradient-operated images. (The smooth, edged-enhanced images are the actual input to the cross-correlation calculation.) The resulting aligned image (**bottom row**) was produced by iterative calculations of the rotational and translational transformations until no significant further changes in the image orientation were obtained.

adjacent sections. We have rejected these approaches because they are time-consuming and subjective. Instead, we have implemented two distinct alignment procedures that rely only on the mathematical properties of the images and are, therefore, objective and automatic. The first procedure is based on the principal axes transformation, and the second involves cross-correlation matching of image features.

For any point in a rigid body, the principal axes transformation determines a set of orthogonal axes (the principal axes) and corresponding principal moments of inertia (*6*). The coronal section image is treated as a rigid body; the nonzero pixels are assigned a value of one and the principal axes are calculated for the center of mass (centroid) of those points. Coincidentally, the principal axis through the coronal section in its longest dimension is formally equivalent to the line of best fit through the image (*7*). Alignment therefore consists of a translation that places the image centroid in the origin of a reference coordinate system and a rotation that makes the longest principal axis coincident with that system's horizontal axis (Fig. 2). Application of the algorithm to the images in a serial set produces a set of images that are in register. The amounts of rotation and translation necessary for alignment are calculated best values; no subjective input is required from the experimenter.

The principal axes method works well for most rat brain coronal sections (*4*). However, if the image is nearly round (principal axes about equal), or if the bilateral symmetry of the image is lacking (for example, in damaged or asymmetric sections), the principal axes alignment may be unsatisfactory. This occurs routinely in about 8 to 12 images in a serial set of 125. Alignment of these problem sections by cross-correlation was suggested by the experience of one of us in an unrelated 3-D reconstruction project (*8*).

The correlation of nonidentical images (cross-correlation) is a measure of their similarity, including the extent to which they are in register (*7, 9, 10*). Cross-correlation is a two-dimensional function in which the location of the maximum is related to the relative translation required to superimpose one image onto the other. Conceptually, one image is held fixed while the second is repositioned (by translations only) to overlay the first in every possible position. At each step, the pixel-by-pixel product of the two images

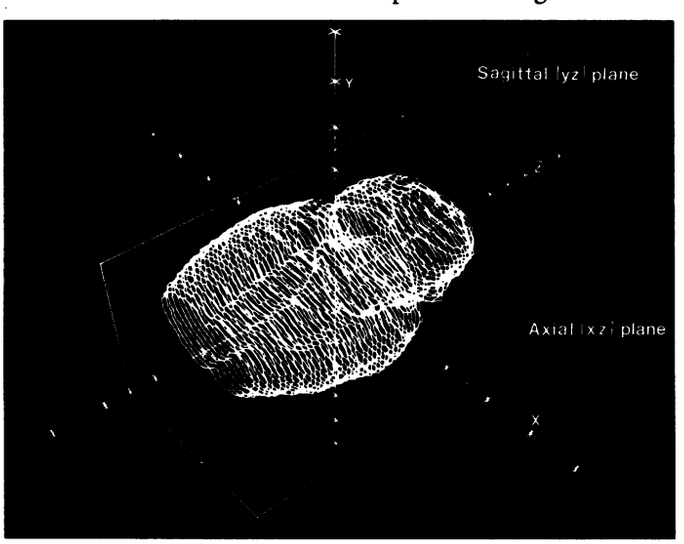

Fig. 5. A reconstruction coordinate system. Shown here is the Cartesian coordinate system in which the 3-D reconstructions are assembled. The coronal images, by definition, lie in planes coincident with, or parallel to, the *xy* plane. The brain envelope shown as contours is that of a "standard serial set" constructed as the mean of 12 normal glucose utilization controls. Reconstructions of experimental data are fully specified by nine degrees of freedom—rotations, translations, and scaling on all three axes. Image alignment fixes five of them (the three rotations, and translations along the *x* and *y* axes) and, because the autoradiographs are all life-size, the *x* and *y* scale factors are 1. Scaling along the *z* axis is proportional to the intersection spacing, and the experimental reconstruction is located along the *z* axis with respect to the "standard" brain as described in the text. Once determined, these nine quantities specify the location of each pixel in this space, and permit the comparison of metabolic data from different reconstructions.

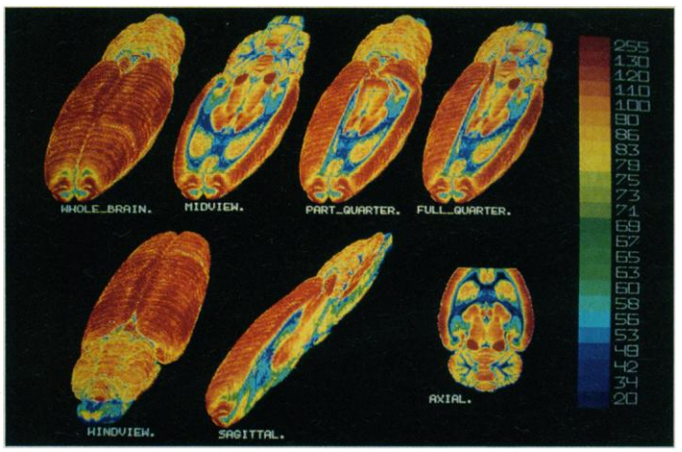

Fig. 6. Representation of whole brain data. Once the individual sections representing a brain set have been aligned, they may be displayed. Here, the whole brain data can be arranged as a stereogram and then cut horizontally, sagittally, or in any combination. All stereogram views distort the anatomy slightly because they are produced by offsetting each serial image by a fixed number of rows and columns, without regard to perspective. More faithful representations of rat brain anatomy can be obtained by direct horizontal (axial image) views obtained after locating the 3-D reconstruction within the reconstruction coordinate system (see text).

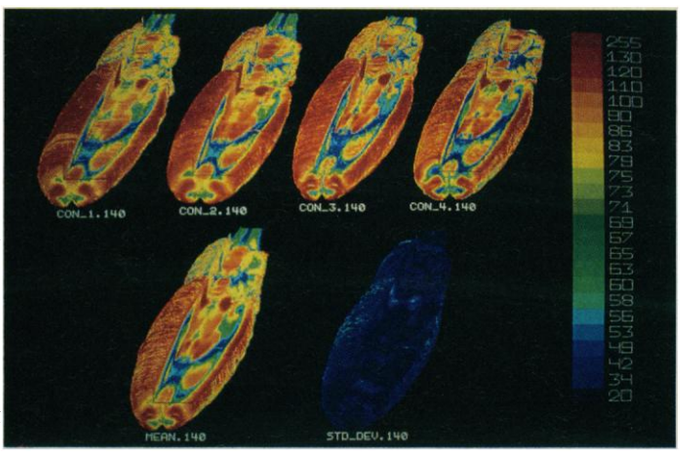

Fig. 7. Several brains can be combined into one "average brain." Because brains from rats of the same age, weight, and sex are highly uniform and differ in overall dimensions by only a few percent, it is possible to put them together, thereby creating an average data set. The creation of average sets involves two steps. First, the individual homologous sections are scaled. There are small size differences on the order of 4 to 8 percent between rat brains. Therefore each image in a set of equivalent images is scaled to the mean height and width of its set. The center of the image is held constant and separate scale factors for the horizontal and vertical directions are applied. After scaling, the assembly of the average brain involves the statistical analysis of homologous pixels. In this way each point can be given a statistical representative such as an average, standard deviation, or standard error. (**Top row**) Four individual brains. These four brains were combined into an average (**bottom lower left**) shown next to an image of the standard deviation.

over the regions of mutual overlap form the values of the cross-correlation. The cross-correlation has its maximum value at that point corresponding to the greatest overlap of both images' features.

In our implementation, cross-correlation is used to compare the edges of high-contrast features in adjacent sections (*11*), rather than the overall image size and shape used by the principal axes method. Because cross-correlation uses more of the information in an image, it is less sensitive to image asymmetry or to the magnitude of section-to-section changes and reliably produces improvements in images inadequately treated by the principal axes method. Further, it can be selectively applied to the undamaged portion of an image to align that image.

Another feature of the cross-correlation method is the necessity of correcting the translational and rotational components of the misalignment in separate steps. Because the two components are coupled such that a change in one simultaneously produces a change in the other, it is necessary to correct the components separately, one at a time. Our program implementation of cross-correlation does this iteratively until no further significant change in the image's orientation is produced. Cross-correlation correction of translational misalignment is illustrated in Fig. 3.

Rotational registration can be effected by cross-correlation because a rotational shift in Cartesian coordinates is equivalent to a

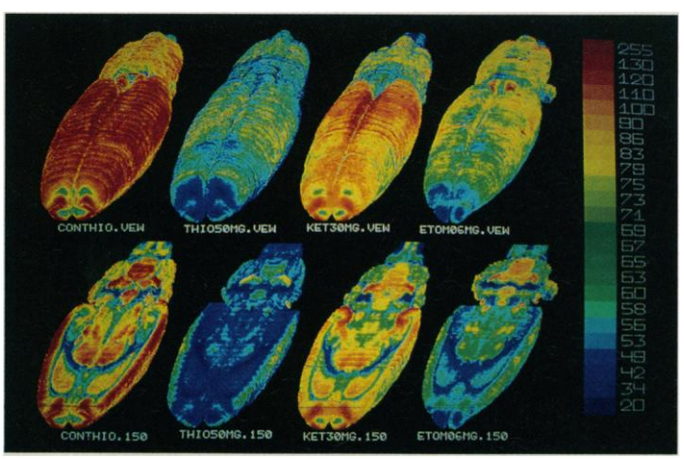

Fig. 8. Anesthetic action on cerebral glucose metabolism. The effect of three separate injectable anesthetics is shown in these stereograms. (**Top row**) Stereograms of whole brains; (**bottom row**) the same brain with the top half removed to reveal internal structures. (**First column**) An unanesthetized control (CONTHIO); (**second column**) the effect of an anesthetic dose of thiopental that depresses brain metabolism in all areas (THIO50MG); (**third column**) the effect of ketamine, a dissociate anesthetic, which depresses brain metabolism in some areas, but causes a stimulatory effect in others, notably the hippocampus (KET30MG); (**fourth column**) the effect of etomidate, an anesthetic which markedly depressed brain metabolism but has its primary effect on the forebrain (ETOM06MG).

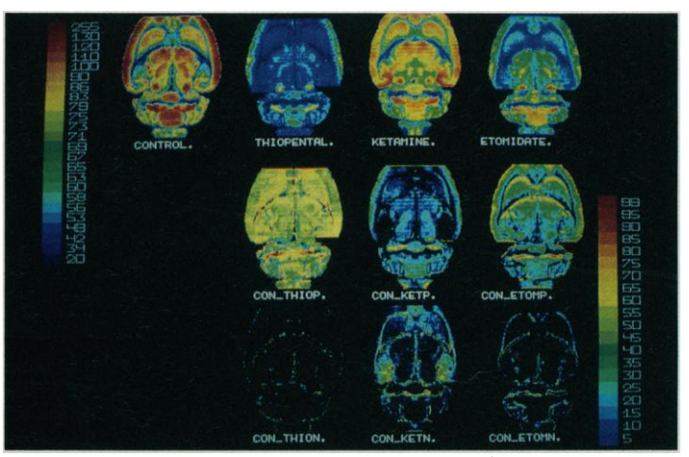

Fig. 9. The effect of the different anesthetics can be compared by subtraction techniques. (**Top row**) Axial views through control, thiopental-, ketamine-, and etomidate-anesthetized rats; the bottom two rows contain pairs of subtraction images: (**middle row**) areas showing a metabolic depression; (**bottom row**) areas where a stimulation of metabolism occurred. Note that the key for the bottom two rows is in units of percent difference.

translational shift in polar coordinates (*10, 12*). Before calculating the cross-correlation function, the coronal section images (both the reference image and the unaligned image) must be resampled in polar coordinates. The polar origin is set at the image centroid (determined previously by the principal axes calculation), and columns of pixel values are determined along rays from the origin at a constant angle increment (Fig. 4). The columns are then arranged vertically and parallel to each other in the manner of a Mercator's projection (Fig. 4, second row). These polar-resampled images are then smoothed and edge-enhanced before the cross-correlation is calculated. The column coordinate of the maximum of the cross-correlation function is directly proportional to the angular component of the misregistration.

In practice, the principal axes alignment is calculated for all the images, with a cross-correlation alignment calculated for those (usually hindbrain) sections that remain obviously misaligned. The principal axes alignment is a relatively inexpensive calculation (20 to 30 CPU-seconds per serial section on a DEC VAX 11/780 computer), whereas cross-correlation is more time consuming (45 to 60 CPU-minutes per section, evaluated with the fast Fourier transform). Cross-correlation alignment usually produces only small adjustments in rotation ($\pm 1.0°$) and translation (± 1 to 2 pixels) for most images aligned by the principal axes method, so that its practical utility is greatest for asymmetric sections.

Assembly of the Aligned Images

The final step in reconstruction is the location of each coronal section image in a defined coordinate system, to reproduce the intersection spacing and to enable the direct comparison of corresponding data from different 3-D data sets. The reconstruction coordinate system is shown in Fig. 5. The coronal sections, by definition, lie in planes parallel to, or coincident with, the *xy* plane. Alignment places the image centroids on the *z* axis with the longer principal axis parallel to the *x* axis. The full specification of the reconstruction involves nine degrees of freedom—a rotation, a translation, and a scaling with respect to each of the three axes. Image alignment fixes five of them (the three rotations and the translations along *x* and *y*), and because the autoradiographs are all life-size, the *x* and *y* scale factors are 1. In addition, the *z* scaling is proportional to the spacing of the sections used to prepare the autoradiographs.

Remaining to be determined is the *z* translation, that is, the movement of the 3-D reconstruction along the *z* axis until it occupies some standard location with respect to the axes. We have chosen to place reconstructions into this coordinate frame such that their outer envelopes maximally overlap with that of a "standard serial set" (Fig. 5), itself constructed as the mean of 12 normal glucose utilization controls. The location of this "standard" 3-D reconstruction was defined as that which places the occulomotor complex at the origin. Essentially, the experimental 3-D reconstruction is translated along the *z* axis by increments, while calculating the sum of the differences squared between *x* coordinates of homologous sets of points at constant *y* along the edges of both envelopes. The best fit is taken as the value of *z* at which the sum of squares is least. Once determined, the *z* translation and the intersection spacing are used to calculate a *z* coordinate for each coronal section. With the coronal sections thus located in the coordinate frame, the reconstructions can be displayed as stereograms (Fig. 6) or resampled in any horizontal or sagittal plane, for display or comparison among different experiments.

The standard brain and the coordinate system defined around it also serve as the basis for a stereotactic atlas of metabolic structures (*13*).

Correspondence of Data in Multiple 3-D Reconstructions

We have used two methods to establish the correspondence of metabolic data, by structure, among separate 3-D data sets. One method [described previously in (*4*)] is to simply assign serial numbers to the images so that images from different serial sets having the same number are taken to represent the same brain section. Serial sets so defined can be compared by matching data, pixel-by-pixel, in equivalent coronal section images. This method was used to prepare the mean and standard deviation reconstructions in Fig. 7.

In general, however, the coronal sections in different serial sets sample the physical brain in different planes, creating an inevitable limit to the accuracy of correspondence. A second method, alluded to above in the description of the determination of the *z* coordinates of images, involves comparisons of horizontal and sagittal images retrieved from experimental data reconstructions. Such images can be located precisely in an image matrix by using the reconstruction coordinates, and comparisons among multiple axial images may be made (see below). In this way, any lack of structural correspondence among the coronal planes of different reconstructions can be overcome by using images in the other planes at right angles to them.

One further correspondence error is related to the uncertainty of the angle at which the coronal sections were cut. That is, there is an uncertainty in the value of the angle made by the coronal section normal and a "true" longitudinal axis, represented in our system by the *z* axis. We assume that this angle has a small value (on the order of a few degrees, because the frozen brain is mounted with respect to a vertical plumb line) and, in fact, treat the reconstructed data as if the angle were zero. The actual out-of-plane uncertainty in the *z* location of the tissue points sampled by autoradiography varies as the product $[(R)\sin(A)]$, where A is the angle made by the coronal plane normal and the "true" longitudinal axis, and R is the distance between a pixel and the image center (at the *z* axis). Obviously, the uncertainty is greatest at the edges of the tissue sections. The value of R for edge points ranges from 5000 μm (in the *y* direction) to 8000 μm (in the *x* direction), and for a 1° angle, the out-of-plane error at a distance of 8000 μm would be 140 μm, or an error on the order of the section spacing. Further, we can assume that the coronal normal vector is randomly distributed about the *z* axis, with the distribution maximum at the *z* axis. In the worst case, coronal images with the same *z* coordinate may, at the outermost edges, actually sample the brain at locations separated by the equivalent of a few sections. Fortunately, most structures of interest are large relative to such errors, so that direct comparisons appear not to suffer significantly. Nevertheless, even slight errors in correspondence are of concern, and we are currently seeking a solution to this problem.

Some Illustrative Examples

The methods of 3-D reconstruction described above are ideally suited to help evaluate the complex patterns of metabolism seen in drug studies. To illustrate this we have compared three anesthetics: thiopental, ketamine, and etomidate (Fig. 8). Thiopental is a barbiturate anesthetic of short duration. At anesthetic doses it produces a profound decrease in cerebral energy metabolism, as well as causing a decrease in blood pressure, body temperature, and respiratory depression. Ketamine is a dissociative anesthetic that interferes with the perception of pain, but allows some degree of consciousness. Ketamine has no significant effects on blood pressure, temperature, or respiration at anesthetic doses. The imidazole

derivative etomidate is a hypnotic. It can produce a profound decrease in oxygen consumption like barbiturates, but unlike barbiturates it does not interfere significantly with temperature regulation, blood pressure, or respiration.

The pattern of metabolic changes produced by these various anesthetics was dramatically different (Fig. 8). Thiopental depressed energy metabolism throughout the entire brain to a similar extent. Ketamine, on the other hand, caused almost no change in CMRglc throughout the brain with the exception that metabolism in the entorhinal cortex and hippocampus was markedly elevated. The effect of etomidate was to cause a profound depression of metabolic rate in the forebrain but not so great a change in the hindbrain. Thus etomidate showed a rostral-to-caudal gradient of metabolic depression. Neither etomidate nor ketamine had a significant effect on the brain stem where the regulation of temperature, respiration, and blood pressure occurs.

These same reconstructed brains are displayed as anatomically correct axial views through the brain at the level of the anterior nucleus of the thalamus in Fig. 9. This method of display allows images from different treatment groups to be mathematically compared. In this case, each anesthetic image was compared to the control and the results displayed as either a positive (Fig. 9, middle row) or negative (Fig. 9, bottom row) difference, expressed as a percent of the control. Positive images show those areas that were depressed by the treatment; negative images are areas that are stimulated.

Conclusions and Future Developments

Three-dimensional reconstruction has been applied to biological problems for nearly a century (*14*), and computer 3-D reconstruction was introduced to the neurosciences in the 1970s by Levinthal and his colleagues (*15*). Their CARTOS system provided for the 3-D display of manually aligned serial images and served as the model for many other systems since then (*16*). More recently, computer image processing has been used for the display and analysis of autoradiographic and histochemical data derived from computer microdensitometry (*17*). The system we have described does not require the intensive manual labor of the earlier ones. The work of reconstruction is done almost entirely by the computer with a minimum of operator input and, hence, a minimum of subjective bias. The alignment procedures, which form the foundation of the reconstruction system, have been developed to accurately place sections in register, providing a representation of energy metabolism closely approximating that which occurred in vivo. This, coupled with the ability to combine the image data from several brains and form an "average brain," promises to be a powerful tool for the future. Future developments will probably be in the area of data analysis. For instance, it may be possible for techniques from multivariate statistical analysis such as the principal components analysis, which is so widely employed in the analysis of spectral data obtained with satellites (*18*), to be applied to the image data from several experimental conditions simultaneously. Finally, this system is of general utility, applicable to autoradiograph data from a variety of experiments including those measuring blood flow, metabolite transport, and receptor binding by radiolabeled ligands.

REFERENCES AND NOTES

1. The rate of oxygen consumption would be an ideal measure of steady-state aerobic energy metabolism, but there are several reasons why it cannot be applied to autoradiographic techniques. There are no long-lived radioisotopes of oxygen. Furthermore water, the product of oxidative metabolism, rapidly diffuses away from the site of formation, and when the brain is cut into sections, the water evaporates. A satisfactory alternative is to measure CMRglc. In normal rats, glucose provides nearly all the energy required by the central nervous system, and CMRglc can be taken to be stoichiometrically related to oxygen consumption and energy production.
2. R. A. Hawkins, A. M. Mans, D. W. Davis, J. R. Viña, L. S. Hibbard, *Am. J. Physiol.* **248**, C170 (1985); D. M. Lu, D. W. Davis, A. M. Mans, R. A. Hawkins, *ibid.* **245**, C428 (1983).
3. L. Sokoloff *et al.*, *J. Neurochem.* **28**, 897 (1977).
4. L. S. Hibbard and R. A. Hawkins, *Am. J. Physiol.* **247**, E412 (1984).
5. L. S. Hibbard, "DIANA and INGRID: A User's Guide to Subroutine Libraries for Digital Image ANAlysis and INteractive GRaphics Image Display" (Pennsylvania State University, Hershey, PA, 1984).
6. H. Goldstein, *Classical Mechanics* (Addison-Wesley, Reading, MA, 1950).
7. A. Rosenfeld and A. Kak, *Digital Picture Processing* (Academic Press, New York, 1982).
8. L. S. Hibbard, B. J. Dovey-Hartman, R. B. Page, *Comput. Biomed. Res.* **16**, 411 (1986).
9. R. C. Gonzalez and P. Wintz, *Digital Image Processing* (Addison-Wesley, Reading, MA, 1977).
10. W. K. Pratt, *Digital Image Processing* (Wiley-Interscience, New York, 1978).
11. P. E. Anuta, *IEEE Trans. Geosci. Electron.* **8**, 353 (1970); J. Moik, *NASA SP-431* (1980).
12. W. K. Pratt, *IEEE Trans. Aerosp. Electron. Syst.* **10**, 353 (1974).
13. L. S. Hibbard, J. S. McGlone, R. A. Hawkins, *Soc. Neurosci. Abstr.* **11**, 1090 (1985); J. S. McGlone, L. S. Hibbard, R. A. Hawkins, R. Kasturi, *IEEE Trans. Biomed. Eng.*, in press.
14. P. M. Gaunt and W. A. Gaunt, *Three-Dimensional Reconstruction in Biology* (University Park Press, Baltimore, MD, 1978).
15. E. R. Macagno, C. Levinthal, I. Sobel, *Annu. Rev. Biophys. Bioeng.* **8**, 323 (1979); C. Levinthal, E. Macogno, C. Tountas, *Fed. Proc. Fed. Am. Soc. Exp. Biol.* **33**, 2336 (1974); C. Levinthal and R. Ware, *Nature (London)* **236**, 207 (1972).
16. E. K. Fram and S. L. Young, *Fed. Proc. Fed. Am. Soc. Exp. Biol.* **43**, 327 (1984); H. Gras, *Comput. Programs Biomed.* **18**, 217 (1984); A. Stein, S. Juliano, P. Karp, P. Hand, *Neurosci. Methods* **10**, 189 (1984); L. G. Briarty and P. H. Jenkins, *J. Microsc.* **134**, 121 (1984); W. K. Smith, D. S. Schlusselberg, B. G. Culter, D. J. Woodward, *Soc. Neurosci. Abstr.* **9**, 353 (1983); E. M. Johnson and J. J. Capowski, *Comput. Biomed. Res.* **16**, 79 (1983); J. Dorup, G. K. Andersen, A. B. Maunsbach, *J. Ultrastruct. Res.* **85**, 82 (1983); J. W. Sundsten and J. W. Prothero, *Anat. Rec.* **207**, 665 (1983); Y.-M. M. Wong, R. P. Thompson, L. Cobb, T. P. Fitzharris, *Comput. Biomed. Res.* **16**, 580 (1983); F. Afshar and E. Dykes, *J. Neurosurg.* **57**, 491 (1982); S. D. Chawla, L. Glass, S. Freiwald, J. W. Proctor, *Comput. Biol. Med.* **12**, 223 (1982); J. Prothero and J. Prothero, *Comput. Biomed. Res.* **15**, 598 (1982); P. B. Moens and T. Moens, *J. Ultrastruct. Res.* **75**, 131 (1981); J. C. Mazziota and B. L. Hamilton, *Comput. Biol. Med.* **7**, 265 (1981); J. K. Stevens, T. L. Davis, N. Friedman, P. Sterling, *Brain Res. Rev.* **2**, 265 (1980); J. J. Capowski, *Comput. Biomed. Res.* **10**, 617 (1977).
17. G. C. Goochee, W. Rasband, L. Sokoloff, *Ann. Neurol.* **7**, 359 (1980); C. R. Gallistel *et al.*, *Neurosci Biobehav. Rev.* **6**, 409 (1982); T. C. Rainbow, W. V. Bleisch, A. Biegon, B. S. McEwen, *J. Neurosci. Methods* **5**, 127 (1982).
18. F. F. Sabins, Jr., *Remote Sensing—Principles and Interpretation* (Freeman, San Francisco, CA, 1987); R. A. Schowengerdt, *Techniques for Image Processing and Classification in Remote Sensing* (Academic Press, New York, 1983).

19. We thank J. Heisey for expert editorial assistance, M. R. DeJoseph for technical assistance, F. B. Modruson for programming assistance, and A. Mans and R. Kasturi for helpful discussions. Supported by the National Science Foundation (grant BNS8506479), the National Institute of Neurological and Communicative Disorders and Stroke (grants NS16389 and NS16737), the National Institute on Alcohol Abuse and Alcoholism (grant AA06023), and the Whitaker Foundation. Support for this work has also been provided by the Departments of Anesthesia and Radiology, M. S. Hershey Medical Center of the Pennsylvania State University.